Surveys in Geophysics (2025) 46:1059–1078
https://doi.org/10.1007/s10712-025-09910-x

Induced Gravitational Effect and Stress Change by Tsunami Surge

Byeongwoo Kim[1] · Tae-Kyung Hong[1] · Junhyung Lee[1] · Seongjun Park[1] · Jeongin Lee[1]

Received: 24 March 2025 / Accepted: 23 September 2025 / Published online: 3 October 2025

Abstract

Tsunami is the oceanic gravity waves produced by mass displacements in large shallow offshore thrust earthquakes. The January 1, 2024 M_W7.5 Noto Peninsula earthquake excited a tsunami to spread across the East Sea (Sea of Japan), arriving at the east coast of the Korean Peninsula. The influence of oceanic gravity waves on the coastal medium is investigated. The mass loading by tsunami induces ground tilting, producing transient long-period ground motions to be polarized in coastline-perpendicular directions. The tsunami-induced ground motions are well recorded in inland seismometers nearby the coast. The wavetrain durations and spectral contents of the tsunami-induced seismic signals in seismometers share with those of the tsunami waves in tide gauges, suggesting the same source of energy. The amplitudes of tsunami-induced ground motions are proportional to the tsunami heights, being modulated by the distance from the coast and medium properties. The discriminative tsunami-induced ground motions produce dynamic stress changes that are effective at shallow depths, reaching 0.81 kPa on the coast. A large runup height may induce dynamic stress changes effective to depths.

Keywords Noto Peninsula earthquake · Tsunami surge · Tsunami-induced ground motion · Inland deformation · Induced stress change

Article Highlights

- The January 1, 2024 M_W7.5 Noto Peninsula earthquake tsunami induces inland deformation.
- Inland seismographs record tsunami-induced seismic wavetrains that are polarized in coastline-perpendicular directions.
- The gravitational tsunami effect decreases with distance from the coast.

✉ Tae-Kyung Hong
tkhong@yonsei.ac.kr

[1] Department of Earth System Sciences, Yonsei University, 50 Yonsei-ro, Seodaemun-gu, Seoul 03722, South Korea

1 Introduction

Large earthquakes produce strong seismic waves that cause strong ground motions and accompany large mass displacements (Hong et al. 2017; Kim and Hong 2018). Such mass changes excite various gravity waves in the Earth depending on the medium. The gravity waves in solid earth are the elastogravity waves that propagate with a speed of light and are well observed after megathrust earthquakes (Harms et al. 2015; Montagner et al. 2016; Vallée et al. 2017; Hong et al. 2021b). Mass changes in shallow-focus offshore earthquakes produce oceanic gravity waves, tsunamis, that cross the seas (Kanamori 1972; Fukao 1979; Okal 1988; Pelayo and Wiens 1992; Satake 1994; Satake and Tanioka 1999; Synolakis and Okal 2005). Also, the mass change induces acoustic gravity waves that transmit to the atmosphere and cryosphere (Satake 2002; Artru et al. 2005; Hickey et al. 2009; Rolland et al. 2010; McKenzie and Jackson 2012; Hendin and Stiassnie 2013; Coïsson et al. 2015; Bromirski et al. 2017; Nishikawa et al. 2022). The amplitudes of gravity waves increase in low-density atmosphere, incurring ionospheric perturbations (Galvan et al. 2012; Mikumo et al. 2013; Garcia et al. 2014; Yu et al. 2015). However, the effect of gravity waves on the Earth has been poorly investigated.

The amplitude of oceanic gravity wave (tsunami-wave height) does not simply decrease with distance from the source, but increases as it approaches the coasts (Abe 1973; Satake 2002; Baba et al. 2004; Dao and Tkalich 2007; Hayashi 2010). Fault geometry and motion further control tsunami height (Kanamori 1972; Ambraseys 1962; Ward 1980; Ambraseys and Melville 1995; Satake and Tanioka 1999; Levin and Nosov 2009). Thus, the tsunami loading is effective around the coast, varying by azimuth from the source (Pino et al. 2004; Nawa et al. 2007; Kimura et al. 2013; Goto et al. 2021). The volumetric mass loading by tsunami induces ground tilting, producing long-period seismic wavetrains (Wielandt and Forbriger 1999; Yuan et al. 2005; Nishida et al. 2019). However, the gravity-wave effect on the ground deformation and stress loading has been limitedly investigated.

Tsunami waves observed in tide gauges present low-frequency contents with peak frequencies of ~0.001 Hz, which is well distinguished from the dominant frequencies of microseisms (0.05–0.5 Hz) (Gutenberg 1931; Longuet-Higgins 1950; Cessaro 1994; Bromirski and Duennebier 2002; Ardhuin et al. 2012; Park and Hong 2020). Such low-frequency contents make it difficult to assess the influence of oceanic gravity waves on the media. Further, the high-frequency contents of oceanic gravity waves remain unclear (Chelton and Enfield 1986; Woodworth and Player 2003; Holgate et al. 2013; Lee et al. 2022). In this sense, ground motion records with high sampling rates are essential for the study. Ocean-bottom and coastal ground motions during tsunami earthquake may provide the information on the tsunami excitation (Ben-Menahem and Rosenman 1972; Kanamori 1972; Pelayo and Wiens 1992; Todorovska and Trifunac 2001; Merrifield et al. 2005; Okal 2017).

The January 1, 2024 M_W7.5 Noto Peninsula earthquake occurred across the coastline of the Noto Peninsula, producing a tsunami in the East Sea (Fujii and Satake 2024; Heidarzadeh et al. 2024; Yamanaka et al. 2024; Yuhi et al. 2024). The tsunami was well observed in tide gauges off the east coast of the Korean Peninsula. The East Sea (Sea of Japan) provides a natural laboratory with a unique closed ocean environment with tsunamis, which is useful for studying tsunami effects on the coast and inland regions. External forces induce medium deformation (Kobori et al. 1993; Korn 1993; Liu and Dobry 1997; Curtis et al. 2006; Wapenaar and Fokkema 2006; Kennett 2009). We investigate the gravitational influence of the tsunami on the coasts and inland media where the tsunami reaches. Dynamic stress changes

associated with transient deformation are assessed. We examine the influence of the tsunami using seismometers with high sampling rates.

2 Geology and Data

The East Sea (Sea of Japan) is a unique enclosed oceanic environment with earthquakes and tsunamis (Fig. 1a). The East Sea was formed by a paleo-continental rifting in the Oligocene to the mid-Miocene. The paleo-rifting structures are seismogenic under the current stress environment. Moderate-size and large earthquakes occur in these structures at the margins of the East Sea (Choi et al. 2012; Hong et al. 2024; Park and Hong 2024). The ocean depths reach 3.76 km in the East Sea, composing an environment that accommodates tsunamis (Shuto and Matsutomi 1995; Choi et al. 2016; Mulia et al. 2020; Satake et al. 2022). There have been several destructive tsunamis in the East Sea, causing the damage on the east coast of the Korean Peninsula and the western Japanese islands (Satake 1985; Sato et al. 1995; Takahashi et al. 1995; Tanioka et al. 1995; Titov and Synolakis 1997).

The January 1, 2024 M_W7.5 Noto Peninsula earthquake excited tsunami that was observed around the East Sea (Sea of Japan) including the east coast of the Korean Peninsula. The earthquake is a thrust event with a focal depth of 16 km (Chen et al. 2024; Fujii and Satake 2024; Masuda et al. 2024). The fault strike is 213°, and the rake is 79°. The rupture plane lies across the eastern coast of the Noto Peninsula, uplifting the surface by 4.1 m (Chen et al. 2024; Xu et al. 2024; Yang et al. 2024). The rupture-plane size is 130–160 km by 20 km (Ma et al. 2024; Okuwaki et al. 2024; Xu et al. 2024; Yang et al. 2024). The rupture plane is composed of 2–6 segments (Kutschera et al. 2024; Ma et al. 2024; Masuda et al. 2024; Okuwaki et al. 2024; Xu et al. 2024; Yang et al. 2024). The seafloor uplift produced a strong tsunami with a peak height of 6 m in the Joetsu coast of Niigata Prefecture (Yuhi et al. 2024). The tsunami was observed on the western coast of the Japanese islands and the eastern coast of the Korean Peninsula. The tsunami arrived at the east coast of the Korean Peninsula in 1.8 h after the event occurrence (Fig. 1a; Fig. S1 in the supplementary materials).

The average ocean depths from the event to the east coast of the Korean Peninsula are 0.45–1.64 km (Fig. 1a). The northern paths are laid on deeper ocean, while the ocean depth decreases to the south. The expected tsunami phase velocities along the paths are 76–456 km/h. Tide gauges and dense seismic networks are available near the coast of the Korean Peninsula (Fig. 1a). We collect tidal heights from tide gauges that are deployed along the coast of the western East Sea (http://www.khoa.go.kr/oceangrid/koofs/kor/observation/obs%5Freal.do). The sampling rate in tide gauges is 1 min. Additionally, we collect seismic data from two ocean bottom seismometers that are placed near the east coast (Fig. 1a; Fig. S1 in the supplementary materials) (Sohn et al. 2023). We also collect seismic data from 130 broadband stations (89 borehole stations and 41 surface stations) on the Korean Peninsula (Fig. 1). The sampling rate is 0.01 s.

3 Tsunami Waves and Tsunami-Induced Seismic Wave

The January 1, 2024 M_W7.5 Noto Peninsula tsunami approached the Korean Peninsula across the East Sea. The tsunami waves are well observed by tide gauges off the east coast of the Korean Peninsula (Fig. S2 in the supplementary materials). The tsunami waves lasted over 48 h because of continuous tsunami surge on the coast. The tide

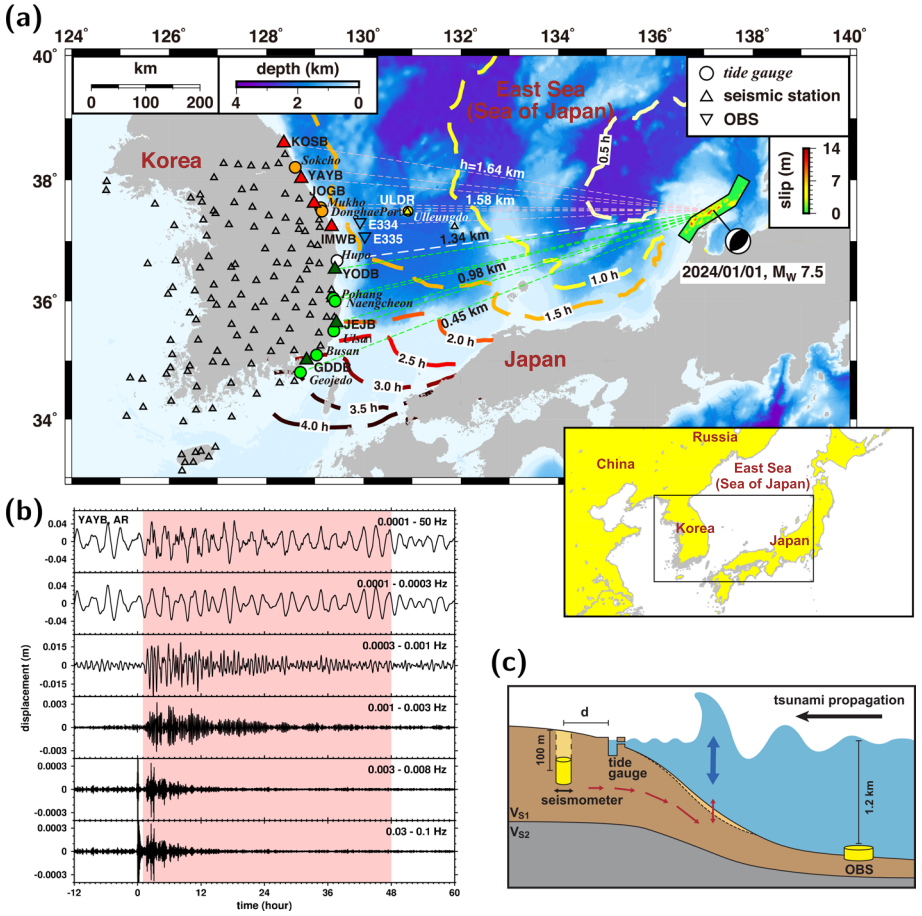

Fig. 1 **a** Map of the January 1, 2024 M_W7.5 Noto Peninsula earthquake and seismic stations (triangles). The rupture model and focal mechanism solution of the earthquake is presented (Xu et al. 2024). The tsunami from the event propagates across the East Sea (Sea of Japan). Temporal tsunami-arrival locations (thick broken lines) and the average ocean depths along paths to stations are presented. The tide gauges around the Korean Peninsula are marked (circles). The study region is marked (inset). **b** Filtered seismic records for various frequency bands. The seismic records are plotted in lapse time after the earthquake origin time (time 0). The filtering frequency bands are indicated. The tsunami-induced signals are marked. The tsunami-induced signals last more than 48 h. **c** Schematic model of tsunami-induced stress loading and coastal deformation. A borehole seismometer, tide gauge and ocean bottom seismometer (OBS) are marked. Coastal region is deformed by the tsunami, inducing transient tsunami-induced seismic signals

gauge measures vertical motions of the sea surface. The peak heights of the tsunami are 0.82 m above the mean sea level. The tsunami reached the east coast at ~332 km/h. In addition, a dispersive feature is apparent in the tsunami wave (Hanson and Bowman 2005; Kubota et al. 2020).

The earthquake excited strong seismic phases with impulsive *P* waves (Fig. S3 in the supplementary materials). The seismic phase records for the earthquake are dominated by surface waves. The seismic wavetrains and surface waves are dominant in ~0.03 to 0.1 Hz for 20 min after the *P* arrival (Fig. 1b; Fig. S3 in the supplementary materials).

Long-period seismic wavetrains persist for over 48 h (Fig. 1b; Fig. S4 in supplementary materials). These long-period waveforms are well observed in borehole stations, while relatively weak in surface stations. The observed seismic wavetrains display longer wavetrains and lower-frequency contents than coda and scattered waves following the major seismic phases (Hong et al. 2005; Hong and Wu 2005). The onset times of long-period wavetrains in the seismometers coincided with tsunami arrivals in nearby tide gauges (Fig. 2a). The wavetrain durations and waveform shapes are similar between the records in seismometers and tide gauges, suggesting the same source of energy. This observation indicates that the tsunami-induced signals may be developed by the tsunami runup on the coast. It is interesting that the tide gauge and seismic station at Ulleungdo (ULDR) in a shorter distance presents a shorter duration (Figs. S2, S4 in the supplementary materials). The observation suggests that tsunami duration increases with distance (Satake and Tanioka 1995; Rabinovich et al. 2006; Rabinovich and Eblé 2015). However, the signals are not apparent in ocean bottom seismometers near the east coast (Fig. 1c; Fig. S1 in the supplementary materials).

The tsunami-induced signals in seismic sensors may be associated with ground deformation by tsunami loading on the coast. Borehole seismograms are useful for observing the tsunami-induced seismic signals, indicating that the influence reaches depths. The tsunami-induced seismic signals are strong in the horizontal components, while rare in

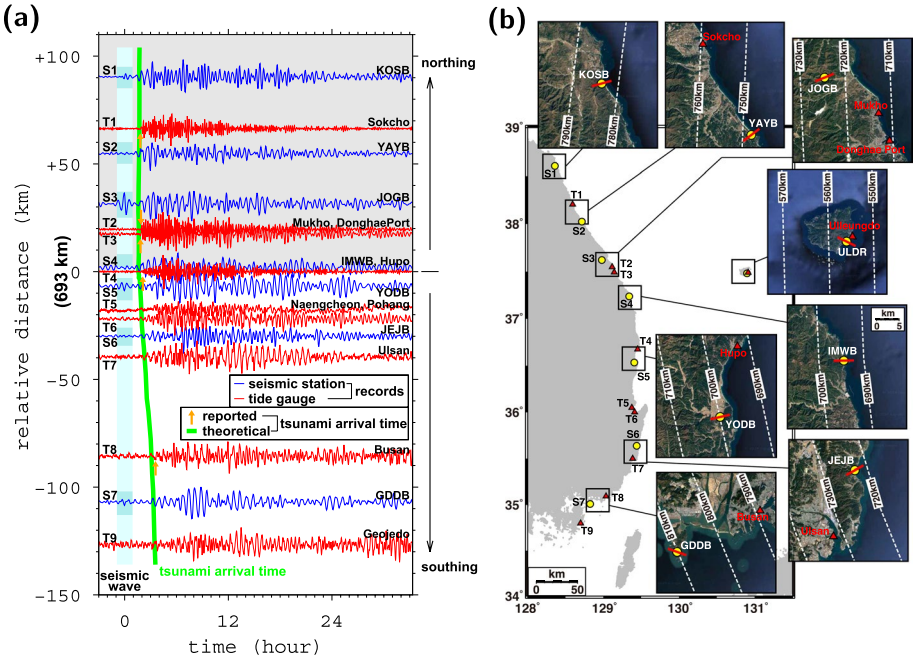

Fig. 2 **a** Record sections in tide gauges and seismic stations. The relative distances are presented. Reported tsunami-arrival times are indicated (arrows). Tsunami-induced seismic signals are consistent with the tsunami records in tide gauges. Tsunami arrivals match the theoretical tsunami traveltime curve (thick solid line). The seismic waves from the earthquake are indicated on the records of seismic stations (shaded waveforms). **b** Polarization directions (solid lines over stations) of tsunami-induced seismic signals at stations KOSB, YAYB, JOGB, ULDR, IMWB, YODB, JEJB and GDDB. The locations of the stations are marked on the map. The polarization directions are nearly perpendicular to the coastline

the vertical component (Fig. 3a). The peak displacement/amplitude ratios of tsunami-induced seismic signals (shaded wavetrains in Fig. 3a) between vertical and horizontal components at eight stations (GDDB, IMWB, JEJB, JOGB, KOSB, ULDR, YAYB, YODB) are 0.012–0.353. We, thus, observe the dominant energy of tsunami-induced seismic signals in the horizontal components, which is consistent with previous studies (Yuan et al. 2005; Nawa et al. 2007; Nishida et al. 2019).

The apparent velocities of tsunami propagation are different between the northern and southern coasts (Fig. 2a). This is because the ocean depths along the paths to the northern coast are deeper than those to the southern coast. The tsunami-arrival times are consistent in the northern paths. In southern paths, apparent tsunami speed among stations is 48 km/h (Fig. 2a).

The waveform correlation of tsunami records between tide gauges at Ulleungdo and Mukho, located along a common great-circle path to the earthquake, presents an arrival time difference of 33 min (Fig. 1a; Fig. S1a in the supplementary materials). The observation suggests the apparent tsunami speed to be ~ 271 km/h, which is faster than the apparent near-offshore tsunami speed (48 km/h) in the southern paths. This is because the ocean depth generally increases with distance from the coast.

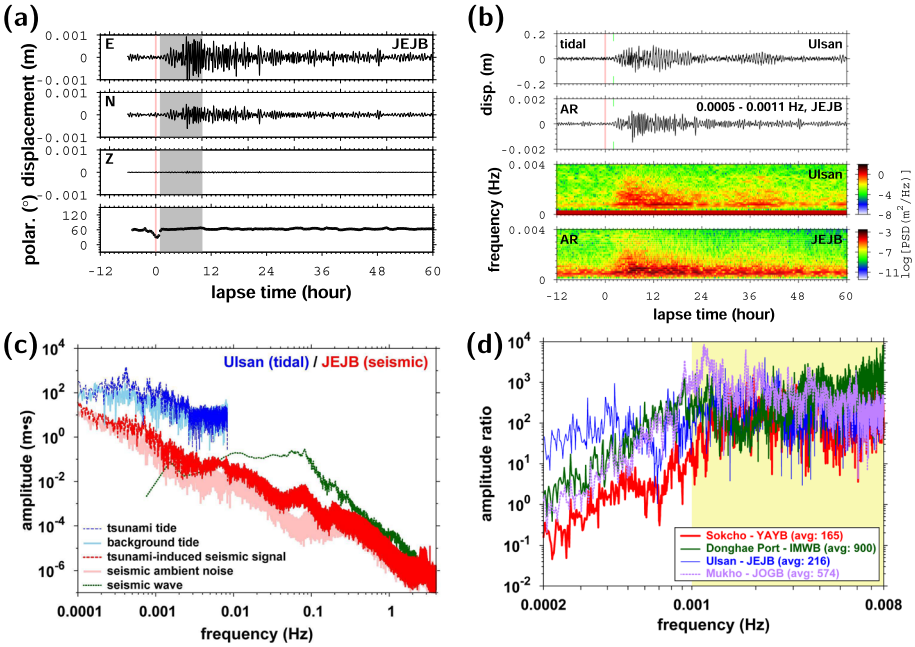

Fig. 3 **a** Three-component tsunami-induced seismic signals and polarization directions at JEJB station. Comparison of **b** waveforms and spectral contents, **c** spectral amplitudes between tsunami records in tide gauge and horizontal (AR) tsunami-induced seismic signals at JEJB seismic station. The tsunami-induced seismic signals in radial directions at 0.0005–0.0011 Hz are observed. The wavetrain durations, shapes and spectral contents are similar between tsunami records in tide gauges and tsunami-induced seismic signals. The spectral amplitudes of ambient noise as well as seismic waves from the earthquake are presented for reference. **d** Spectral amplitude ratios between tsunami waves of tide gauges and horizontal (AR) tsunami-induced seismic signals of adjacent seismic stations YAYB, IMWB, JEJB and JOGB. The spectral amplitude ratios are nearly constant at 0.001–0.008 Hz (shaded range), being 165–900

4 Ground-Motion Polarization

We examine seismic-wave polarization from the earthquake. The *P* phases are polarized in the radial directions from the earthquake to the stations (Fig. S5 in the supplementary materials). We determine the polarization directions of tsunami-induced seismic signals by analyzing ground motions recorded in 1–10 h after the earthquake origin time when major seismic phases from the earthquake have fully passed (Fig. S6 in the supplementary materials). We prepare seismic records bandpass filtered between 0.0005 and 0.0011 Hz, in which tsunami-induced seismic signals are dominant. We determine the apparent polarization direction of the ground motions using eigenvector analysis, with 90-min windows at 20-min intervals.

The strong horizontal ground motions suggest discriminative lateral polarization (Fig. S7 in the supplementary materials). The polarization directions are constant with time but different from the great-circle directions (i.e., *P*-polarization directions) and vary by station locations. The apparent radial directions of tsunami-induced seismic signals are nearly perpendicular to the coastline (Fig. 2b).

Ocean tides and tsunamis approach coastlines perpendicularly (Titov et al. 2005; Dao et al. 2009; Saito 2019). Thus, the polarization directions agree with the tsunami incidence directions to the coast near the stations, suggesting that the tsunami-induced seismic signals are produced by energy incident in coastline-perpendicular directions (Fig. 2b). The apparent radial direction may be modulated by coastline geometry and seafloor topography on the tsunami path. The rotated seismic wavetrains for apparent radial (AR) directions present similar waveforms with the tsunami-wave records in nearby tide gauges (Fig. 3b; Fig. S8 in the supplementary materials). The observations support that the observed wavetrains are produced by the tsunami. The polarization in coastline-perpendicular direction is consistent with previous studies and suggests that the dominant energy may be excited near the coast (Yuan et al. 2005; Hanson and Bowman 2005; Okal 2007; Poplavskiy and Le Bras 2013).

5 Spectral Content

The tsunami-wave height and duration are reflected in the seismic records. The solid earth response function for the tidal loading may be reflected in the tsunami-induced signals. The energy transfer from tsunami to tsunami-induced seismic signals may be dependent on the local geological properties and subsurface structures. Thus, the spectral contents of tsunami-induced seismic signals may present the nature of tsunami waves and tsunami-loading effect.

In the frequency band of 0.001–0.008 Hz, the spectral contents of horizontal tsunami-induced seismic signals in seismic stations are similar to those of tsunami waves in tide gauges (Fig. 3c). Also, the tsunami-induced seismic signals are distinguished from the ambient noise and seismic phases in the frequency contents (Fig. 3c). The observation suggests that the tsunami-induced seismic signals may share the spectral contents with the tsunami waves in the tide gauges (Fig. 3c, Fig. S9 in the supplementary materials). The similar frequency contents are further supported by similar wavetrain duration (Fig. 3b; Fig. S8 in the supplementary materials).

The tsunami-induced seismic signals may present clear higher-frequency contents than the tsunami waves recorded on the sea surface. This may be partly because seismic sensors cover a wide frequency band and tide gauges are limited by low sampling rates (1 sample per minute). It is noteworthy that local atmospheric pressure changes may cause sea surface disturbance additionally (Janssen 2004; Ardhuin et al. 2007; Hanley et al. 2010; Lee et al. 2010; Oh and Jeong 2013).

The seismic waves are dominant in frequencies of 0.01–1 Hz. The tsunami-induced seismic signals partly overlap with the seismic waves at frequencies of 0.002–0.008 Hz in the horizontal components, sharing the upper corner frequencies of ~0.1 Hz (Fig. 3c). Core-reflected seismic phases and surface waves traveling around the major and minor arcs of the Earth may be partly included in the later wavetrains (Fig. S10 in the supplementary materials). In frequencies of > 0.02 Hz, the wavetrains may be dominantly affected by the late-arrival seismic phases. The apparent difference in frequency contents suggests that the tsunami waves may have distinct frequency contents.

We estimate the amplitude ratios between the tsunami wave in tide gauges and horizontal (AR) tsunami-induced seismic signals at 0.0002–0.008 Hz where tsunami waves are most dominant (Fig. 3d). The amplitude ratios remain constant at 0.001–0.008 Hz, varying between 165 and 900 by station (Fig. 3d). The similar spectral contents suggest that tsunami pressure on the seafloor induces ground tilting. The consistent spectral contents suggest that the tsunami-induced waves are originated from the same source with similar attenuation. Also, the tsunami pressure on the seafloor may be dominant in the frequencies.

6 Coastal-Medium Deformation

Long-period tsunami loading produces tsunami-induced seismic signals, suggesting long-period medium deformation that is effectively observed at the borehole seismometers near the coast. We estimate the ratios (R) between the average wavetrain amplitudes after the earthquake and those before the earthquake (Fig. 4a) to infer the discriminative influence of the tsunami. The analyzed wavetrain records before and after the earthquake is 5-h-long. The average amplitude ratios are strong in horizontal directions along the east coast of the peninsula.

The tsunami-induced seismic signals are strong along the coast, decaying rapidly with distance (Fig. 4a). The tsunami-induced seismic signals are hardly observed in inland regions, $>\sim$ 13 km away from the coast. The observation suggests that the medium deformation by the tsunami loading is a local effect near the coast. Similarly, ocean tides may be effective near the coast as well, inducing strong energy in the horizontal components.

It is intriguing to note that the tsunami-induced seismic signals are only effective on the coast, while weak in offshore regions. We hardly observe the tsunami-induced seismic signals in the ocean bottom seismometers on the seafloor, 55 km off the coast (Fig. 1a; Fig. S1 in the supplementary materials). This may be because the tsunami runup height increases due to the seafloor slope as the tsunami-wave approaches the coast. On the other hand, the tsunami waves height changes relatively little in the ocean center. It is noteworthy that the seismic station at Ulleungdo (ULDR) presents lower amplitudes than the stations in the coast. The tsunami height may be mainly controlled by the bathymetry, distance and the source geometry, being modulated by environmental factors on the paths (Synolakis 1987; Tadepalli and Synolakis 1994; Satake and Tanioka 1995; Titov and Synolakis 1998; Okal and Synolakis 2003; Rabinovich et al. 2006; Rabinovich and Eblé 2015).

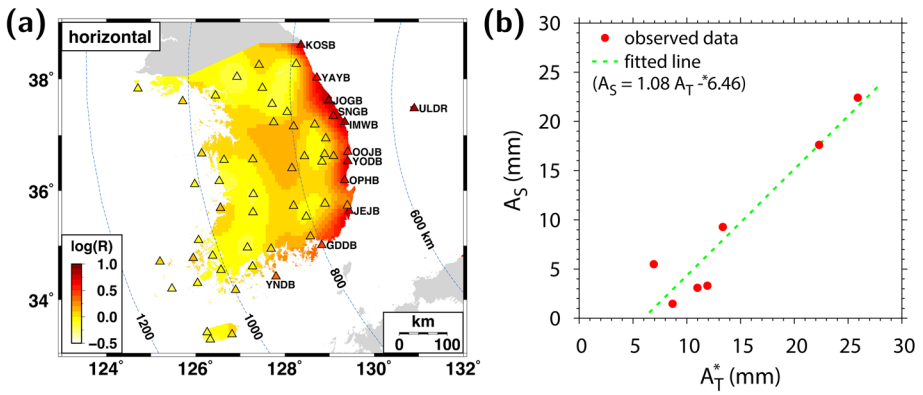

Fig. 4 **a** Amplitude ratios (R) between horizontal (AR) wavetrains after the earthquake and those before the earthquake. The analyzed wavetrain records before and after the earthquake are 5-h-long. The amplitude ratios are large near the east coast of the peninsula. **b** Comparison between horizontal (AR) tsunami-induced seismic signal amplitudes (A_S) and converted tsunami-wave amplitudes (A_T^*) at seismic stations GDDB, IMWB, JEJB, JOGB, KOSB, YAYB and YODB. The tsunami-induced seismic signal amplitudes present a linear relationship with the converted tsunami amplitudes

The effective vertical pressure loading along the coast by the tsunami surge may induce long-period coastline-perpendicular ground tilting and recovery, producing coastline-perpendicular ground motions (Yuan et al. 2005; Boudin et al. 2013; Kimura et al. 2013; Nishida et al. 2019). It is noteworthy that seismometers experience a transient change in the projected gravitational acceleration on the sensor axes plane during the ground tilting by tsunami runup (Wielandt 2002; Graizer 2006). For a ground tilting angle of θ, the apparent acceleration on the horizontal plane is modulated by $\sin\theta$. This modulation factor is approximated to be θ for a small ground tilting angle. On the other hand, the gravitational acceleration on the vertical component is modulated by $(1-\cos\theta)$ that is approximated to be $\theta^2/2$ in the second-order polynomial expansion. Since θ is typically very small (on the order of microradians to milliradians), the vertical modulation factor is close to zero. Thus, the tsunami-induced seismic signals are mainly recorded in the horizontal components, while rarely in the vertical component (Wielandt and Forbriger 1999; Webb 2002; Yuan et al. 2005; Kinoshita 2008). The feature is supported by tiltmeter observations (Boudin et al. 2013; Nishida et al. 2019). Also, we observe that the tsunami-induced signals are much strong at borehole stations, suggesting that ground tilting caused by vertical tsunami mass loading may be a major source mechanism.

We determine the relationship between the amplitude of tsunami-induced seismic signals in seismometers and those of tsunami waves in tide gauges. The tsunami waves are coupled with seismic signals due to tidal loading on the coast. The tsunami-induced seismic signals may be similar to plane waves from a line source, decaying with the square root of distance ($\sqrt{d}$ in Fig. 1c). The tsunami-induced ground motions are dominant in the Earth surface that are influenced by near surface medium properties. The near surface site effect is controlled by the average shear wave velocity within the upper 30 m depth (V_{S30})

(Borcherdt 1994; Boore and Atkinson 2008; Laurendeau et al. 2013; Boore et al. 2014; Seyhan and Stewart 2014; Stewart et al. 2020; Aaqib et al. 2021).

We consider the amplitude of horizontal (AR) tsunami-induced seismic signal at distance d (m) from the coast (A_S) as

$$\begin{aligned} A_S &= E_1 \frac{\sqrt{d_{ref}}}{\sqrt{d}} \left(\frac{V_{ref}}{V_{S30}} \right)^n A_T + E_2, \\ &= E_1 A_T^* + E_2, \end{aligned} \tag{1}$$

where V_{ref} is reference V_{S30} value, n is a constant factor, and d_{ref} is the reference distance. E_1 and E_2 are constants, and A_T^* is the converted tsunami amplitude modulated by distance (d) and site effect (V_{S30}). We use the V_{S30} values at the seismic stations from a national V_{S30} model (Kim and Hong 2022). Also, we set V_{ref} to be 760 m/s, d_{ref} to be 1 m, and n to be 0.7 (Choi and Stewart 2005; Boore and Atkinson 2008; Boore et al. 2014; Stewart et al. 2020).

We find a linear relationship between the amplitudes of tsunami-induced seismic signals and converted tsunami amplitude (A_T^*) (Fig. 4b):

$$A_S = 1.08 A_T^* - 6.46. \tag{2}$$

Additional description of the linear relationship determination is presented in the supplementary materials

7 Dynamic Stress Change and Seismicity Induction

Dynamic stress change may play important role in seismicity induction (Hill and Prejean 2007; Van der Elst and Brodsky 2010). Strong ground motions from large events may trigger earthquakes (Belardinelli et al. 2003; Hong et al. 2018). The 2011 M_W9.0 Tohoku–Oki megathrust earthquake dynamically triggered a series of earthquakes on the Korean Peninsula (Houng et al. 2016). The peak dynamic stress changes during the 2011 Tohoku-Oki earthquake were ~100 to ~400 kPa on the Korean Peninsula (Houng et al. 2016). The dynamic stress changes required for earthquake triggering are different by region depending on the seismotectonic properties, e.g., >~ 0.1 kPa and >~ 30 kPa (Van der Elst and Brodsky 2010; Miyazawa et al. 2021; Takeda et al. 2024).

We estimate the dynamic stress change induced by seismic waves from the earthquake using the peak ground velocities of seismic wavetrains in 1-h time window after the event origin (Fig. S11 in the supplementary materials) (Hill and Prejean 2007; Hong et al. 2016, 2020). We estimate the dynamic stress changes caused by the tsunami-induced seismic signals in 5-h-long waveform records. In order to minimize the influence of seismic phases from the earthquake, we analyze the waveform records in 3–8 h after the earthquake origin time where the tsunami-induced seismic signals are evident (Fig. 5; Fig. S12 in the supplementary materials).

The tsunami-induced seismic signals are bandpass filtered between 0.0005 and 0.0011 Hz to estimate the dynamic stress change. For comparison, we prepare seismic-wave record sections bandpass filtered between 0.0003 and 0.1 Hz to estimate the dynamic stress change induced by the seismic waves from the earthquake. The dynamic stress changes are estimated using a 15-min-long moving time window for both horizontal and vertical components (Fig. 5; see also the supplementary materials).

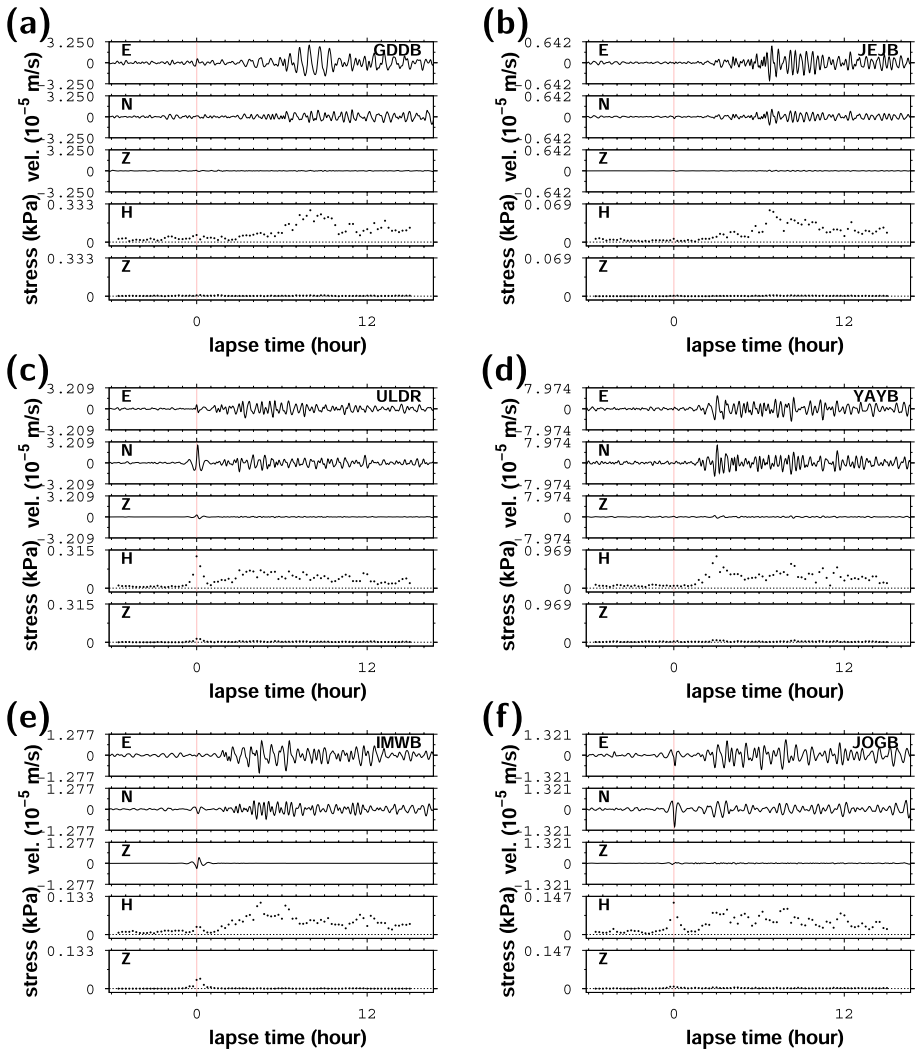

Fig. 5 Tsunami-induced seismic signals and dynamic stress changes at stations **a** GDDB, **b** JEJB, **c** ULDR, **d** YAYB, **e** IMWB, and **f** JOGB. Horizontal wavetrains present tsunami-induced seismic signals, inducing dynamic stress changes

The maximum peak dynamic stress changes induced by the seismic waves from the earthquake are 68 kPa (horizontal) and 39 kPa (vertical) (Fig. 6a; Fig. S13 in the supplementary materials). The dynamic stress change decreases with distance. We, however, do not find any apparent triggered earthquakes on the Korean Peninsula after the earthquake.

It is known that tides also induce earthquakes (Heaton 1975; Tanaka et al. 2002; Bucholc and Steacy 2016; Yan et al. 2023). We examine the seismicity change during the tsunami surge. Continuous long-period deformation for more than 48 h induces long dynamic stress changes in the medium. We assess the dynamic stress change from the tsunami-induced

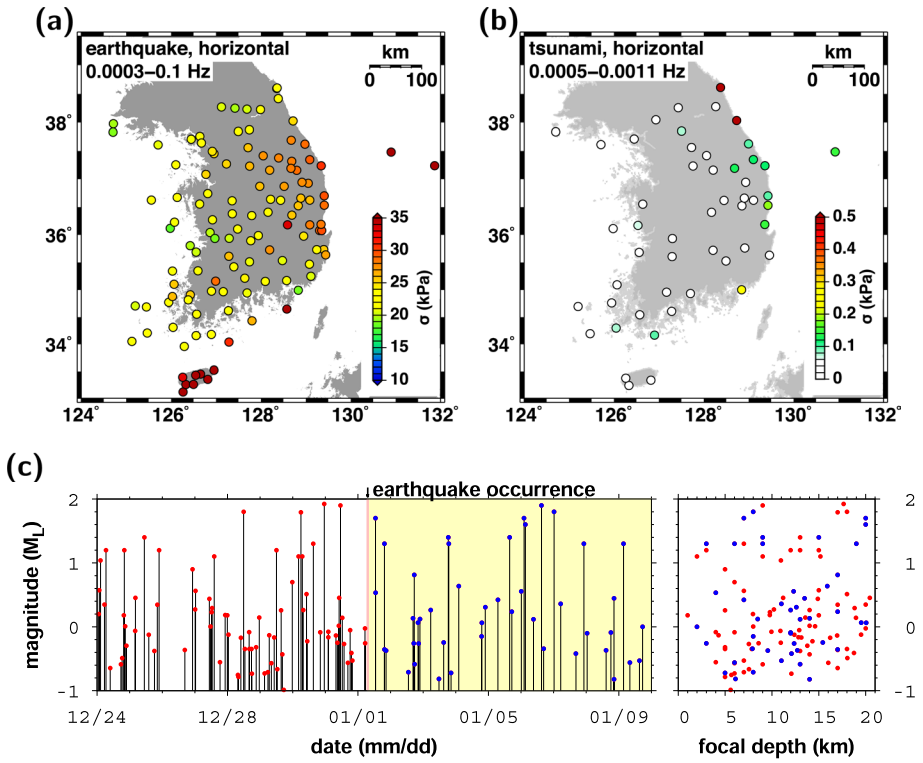

Fig. 6 Spatial variations of peak dynamic stress changes in horizontal direction by **a** seismic wavetrains at 0.0003−0.1 Hz and **b** tsunami-induced signal at 0.0005−0.0011 Hz. The strengths of tsunami-induced seismic signals are relatively large along the east coast. **c** Earthquake occurrence history in the Korean Peninsula. The seismicity presents no apparent changes after the earthquake

seismic signals (Figs. 5, 6(b); Fig. S12 in the supplementary materials). Tsunami loading may induce dynamic stress changes affecting around the coast.

The peak dynamic stress changes by the tsunami-induced seismic signals reach ~ 0.81 kPa around the east coast of the Korean Peninsula (Fig. 6b). The induced dynamic stress changes are much less than the dynamic stress change by seismic waves from the earthquake but still within thresholds for trigger earthquake in active tectonic regions (Van der Elst and Brodsky 2010; Takeda et al. 2024).

We observe some earthquakes in near-offshore regions before and after the Noto Peninsula earthquake and tsunami, with magnitudes M_L − 1 to 2 at depths < 21 km, mostly 5–15 km (Fig. 6c; Fig. S14 in the supplementary materials). The tsunami runup loads pressure on the surface. Thus, the effective dynamic stress change may decrease with depth. Such dynamic stress may induce the earthquakes in the shallow depth effectively. We examine the focal depth distribution before and after the 2024 Noto Peninsula earthquake to determine the influence of tsunami-induced stress perturbation on seismicity. We rarely find apparent focal depth changes after the tsunami arrival, which is consistent with previous studies (Hong et al. 2021a; Park

et al. 2023). The seismicity after the tsunami arrivals is rarely observed, suggesting that the dynamic stress changes are not enough to induce seismicity in the offshore and inland regions.

8 Discussion and Conclusions

Mass displacements develop various gravity waves depending on the medium type. Shallow-focus offshore thrust earthquakes may generate oceanic gravity waves, tsunamis, which are amplified near the coasts. Such local wave amplification and long-period oceanic mass loading for > 48 h may induce discriminative stress around the coast. We investigated the influence of tsunami loading and coastal medium deformation in the region by the 2024 Noto earthquake tsunami. The closed ocean environment in the East Sea composes a natural experiment to examine the tsunami effect.

We analyzed both tsunami-wave records in tide gauges and seismic records in seismometers in the Korean Peninsula. Tsunami-induced seismic wavetrains could be identified from comparisons with tsunami waves in tide gauges. The tsunami-induced seismic signals are well monitored in borehole seismometers near the coast that are less affected by ambient noise on the surface. The observations suggest that seismic records may be used to assess the tsunami-induced medium deformation and effective spatial range over a wide frequency band.

Tsunamis and tides are incident to the coasts in coastline-perpendicular directions. Vertical oceanic mass loading or unloading on the coast by tsunami incidence causes lateral extension or contraction in medium at effective distance. Such tsunami effects make the tsunami-induced seismic signals to be long-period horizontal wavetrains that are polarized in the coastline-perpendicular directions. Thus, tsunami-induced basement deformation is effective in horizontal directions, but weak in the vertical direction. The tsunami effect is strong near the coast, being proportional to the tsunami-wave height.

The tsunami-induced seismic signals are barely observed in inland regions. The amplitude of tsunami-induced seismic signal decreases with distance from the coast, being additionally modulated by medium properties. The tsunami-induced seismic signals share spectral content with tsunami waves in tide gauges. We find strong correlation between tsunami heights and tsunami-induced seismic signal amplitudes, allowing us to infer unknown tsunami heights from observed tsunami-induced seismic signal amplitudes at seismometers.

The long-period tsunami-induced seismic energy dynamically deforms the medium, with deformation decreasing inland. Thus, the tsunami discriminatively deforms the coastal medium, inducing long-period dynamic stress changes. The vertical loading by tsunami runup is applied on the surface. Thus, the dynamic stress change induced by the tsunami-induced seismic signals may decrease with increase in depth. The tsunami-induced seismic signals at borehole seismometers may be useful to assess the induced stress at shallow depths.

The coastal regions experience discriminative transient deformation by the tsunami. The 2024 Noto earthquake tsunami produced 0.81 kPa dynamic stress change on the east coast of the Korean Peninsula, insufficient to trigger earthquakes at seismogenic depths. In turn, we hardly find seismicity changes in seismic zones near the coast where the dynamic stress change induced by the tsunami runup is effective. A large tsunami wave may induce measurable dynamic stress changes at depths, which may trigger earthquakes at faults in critical condition.

Seismic networks effectively detect the oceanic gravity waves and the coastal medium deformation. Seismic stations along the coast may be used to detect ground deformation induced by tsunamis. The tsunami-induced seismic signals are useful for studying the tsunami properties and medium deformation. The strong waveform correlation between tsunami-wave records in tide gauges and tsunami-induced seismic signals in seismic stations suggests that coastal seismometers can be a complement to tide gauges for real-time tsunami monitoring.

Supplementary Information The online version contains supplementary material available at https://doi.org/10.1007/s10712-025-09910-x.

Acknowledgements We thank Drs. Dapeng Zhao (associate editor), Tae-Seob Kang and two anonymous reviewers for constructive review comments. This work was supported by the Korea Meteorological Administration Research and Development Program under grant KMI2022-00710. Additionally, this research was partly supported by the Basic Science Research Program of National Research Foundation of Korea (RS-2017-NR023048).

Declarations

Conflict of interest The authors declare that they have no conflict of interest.

References

Aaqib M, Park D, Adeel MB, Hashash YM, Ilhan O (2021) Simulation-based site amplification model for shallow bedrock sites in Korea. Earthq Spectra 37(3):1900–1930. https://doi.org/10.1177/8755293020981984

Abe K (1973) Tsunami and mechanism of great earthquakes. Phys Earth Planet Int 7(2):143–153. https://doi.org/10.1016/0031-9201(73)90004-6

Ambraseys NN (1962) Data for the investigation of the seismic sea-waves in the eastern mediterranean. Bull Seismol Soc Am 52(4):895–913. https://doi.org/10.1785/BSSA0520040895

Ambraseys NN, Melville CP (1995) Historical evidence of faulting in Eastern Anatolia and Northern Syria. Ann Geophys 38(3–4):1. https://doi.org/10.4401/ag-4110

Ardhuin F, Herbers THC, Watts KP, van Vledder GP, Jensen R, Graber HC (2007) Swell and slanting-fetch effects on wind wave growth. J Phys Oceanogr 37(4):908–931. https://doi.org/10.1175/JPO3039.1

Ardhuin F, Balanche A, Stutzmann E, Obrebski M (2012) From seismic noise to ocean wave parameters: general methods and validation. J Geophys Res Oceans 117(C5):1. https://doi.org/10.1029/2011JC007449

Artru J, Ducic V, Kanamori H, Lognonne P, Murakami M (2005) Ionospheric detection of gravity waves induced by tsunamis. Geophys J Int 160(3):840–848. https://doi.org/10.1111/j.1365-246X.2005.02552.x

Baba T, Hirata K, Kaneda Y (2004) Tsunami magnitudes determined from ocean-bottom pressure gauge data around Japan. Geophys Res Lett 31(8):1. https://doi.org/10.1029/2003GL019397

Belardinelli ME, Bizzarri A, Cocco M (2003) Earthquake triggering by static and dynamic stress changes. J Geophys Res Solid Earth 108(B3):2135. https://doi.org/10.1029/2002JB001779

Ben-Menahem A, Rosenman M (1972) Amplitude patterns of tsunami waves from submarine earthquakes. J Geophys Res 77(17):3097–3128. https://doi.org/10.1029/JB077i017p03097

Boore DM, Atkinson GM (2008) Ground-motion prediction equations for the average horizontal component of PGA, PGV, and 5%-damped PSA at spectral periods between 0.01 s and 10.0 s. Earthqu spectra 24(1):99–138. https://doi.org/10.1193/1.2830434

Boore DM, Stewart JP, Seyhan E, Atkinson GM (2014) Nga-west2 equations for predicting PGA, PGV, and 5% damped PSA for shallow crustal earthquakes. Earthq Spectra 30(3):1057–1085. https://doi.org/10.1193/070113EQS184M

Borcherdt RD (1994) Estimates of site-dependent response spectra for design (methodology and justification). Earthq Spectra 10(4):617–653. https://doi.org/10.1193/1.1585791

Boudin F, Allgeyer S, Bernard P, Hébert H, Olcay M, Madariaga R, El-Madani M, Vilotte J-P, Peyrat S, Nercessian A, Schurr B, Esnoult M-F, Asch G, Nunez I, Kammenthaler M (2013) Analysis and modelling of Tsunami-induced tilt for the 2007, $M = 7.6$, Tocopilla and the 2010, $M = 8.8$ Maule earthquakes, Chile, from long-base tiltmeter and broadband seismometer records. Geophys J Int 194(1):269–288. https://doi.org/10.1093/gji/ggt123

Bromirski PD, Duennebier FK (2002) The near-coastal microseism spectrum: spatial and temporal wave climate relationships. J Geophys Res Solid Earth 107(B8):1. https://doi.org/10.1029/2001JB000265

Bromirski PD, Chen Z, Stephen RA, Gerstoft P, Arcas D, Diez A, Aster RC, Wiens DA, Nyblade A (2017) Tsunami and infragravity waves impacting Antarctic ice shelves. J Geophys Res Oceans 122(7):5786–5801. https://doi.org/10.1002/2017JC012913

Bucholc M, Steacy S (2016) Tidal stress triggering of earthquakes in southern California. Geophys J Int 205(2):681–693. https://doi.org/10.1093/gji/ggw045

Cessaro RK (1994) Sources of primary and secondary microseisms. Bull Seismol Soc Am 84(1):142–148. https://doi.org/10.1785/BSSA0840010142

Chang SJ, Baag CE (2006) Crustal structure in southern Korea from joint analysis of regional broadband waveforms and travel times. Bull Seismol Soc Am 96(3):856–870. https://doi.org/10.1785/012004016 5

Chelton DB, Enfield DB (1986) Ocean signals in tide gauge records. J Geophys Res Solid Earth 91(B9):9081–9098. https://doi.org/10.1029/JB091iB09p09081

Chen GQ, Wu YQ, Xia MY, Li ZY (2024) Focal mechanics and disaster characteristics of the 2024 M 7.6 Noto Peninsula Earthquake, Japan. Front Struct Civ Eng 18(9):1378–1387. https://doi.org/10.1007/s11709-024-1111-1

Choi Y, Stewart JP (2005) Nonlinear site amplification as function of 30 m shear wave velocity. Earthq Spectra 21(1):1–30. https://doi.org/10.1193/1.1856535

Choi H, Hong T-K, He X, Baag C-E (2012) Seismic evidence for reverse activation of a paleo-rifting system in the east sea (sea of Japan). Tectonophysics 572–573:123–133. https://doi.org/10.1016/j.tecto.2011.12.023

Choi BH, Cho YS, Yoon SB (2016) Tsunami research in Korea. Nat Hazards 84:437–454. https://doi.org/10.1007/s11069-016-2439-1

Coïsson P, Lognonne P, Walwer D, Rolland LM (2015) First tsunami gravity wave detection in ionospheric radio occultation data. Earth Space Sci 2(5):125–133. https://doi.org/10.1002/2014EA000054

Curtis A, Gerstoft P, Sato H, Snieder R, Wapenaar K (2006) Seismic interferometry-turning noise into signal. Lead Edge 25(9):1082–1092. https://doi.org/10.1190/1.2349814

Dao MH, Tkalich P (2007) Tsunami propagation modelling-a sensitivity study. Nat Hazard 7(6):741–754. https://doi.org/10.5194/nhess-7-741-2007

Dao MH, Tkalich P, Chan ES, Megawati K (2009) Tsunami propagation scenarios in the south China sea. J Asian Earth Sci 36(1):67–73. https://doi.org/10.1016/j.jseaes.2008.09.009

Fujii Y, Satake K (2024) Slip distribution of the 2024 Noto Peninsula earthquake (M_JMA 7.6) estimated from tsunami waveforms and GNSS data. Earth Planets Space 76(1):44. https://doi.org/10.1186/s40623-024-01991-z

Fukao Y (1979) Tsunami earthquakes and subduction processes near deep-sea trenches. J Geophys Res Solid Earth 84(B5):2303–2314. https://doi.org/10.1029/JB084iB05p02303

Galvan DA, Komjathy A, Hickey MP, Stephens P, Snively J, Song YT, Butala MD, Mannucci AJ (2012) Ionospheric signatures of Tohoku-Oki tsunami of March 11, 2011: model comparisons near the epicenter. Radio Sci 47(04):1–10. https://doi.org/10.1029/2012RS005023

Garcia RF, Doornbos E, Bruinsma S, Hebert H (2014) Atmospheric gravity waves due to the Tohoku-Oki tsunami observed in the thermosphere by Goce. J Geophys Res Atmos 119(8):4498–4506. https://doi.org/10.1002/2013JD021120

Goto K, Ishizawa T, Ebina Y, Imamura F, Sato S, Udo K (2021) Ten years after the 2011 Tohoku-Oki earthquake and tsunami: geological and environmental effects and implications for disaster policy changes. Earth Sci Rev 212:103417. https://doi.org/10.1016/j.earscirev.2020.103417

Graizer V (2006) Tilts in strong ground motion. Bull Seismol Soc Am 96(6):2090–2102. https://doi.org/10.1785/0120060065

Gutenberg B (1931) Microseisms in north America. Bull Seismol Soc Am 21(1):1–24. https://doi.org/10.1785/BSSA0210010001

Hanley KE, Belcher SE, Sullivan PP (2010) A global climatology of wind–wave interaction. J Phys Oceanogr 40(6):1263–1282. https://doi.org/10.1175/2010JPO4377.1

Hanson JA, Bowman JR (2005) Dispersive and reflected tsunami signals from the 2004 Indian ocean tsunami observed on hydrophones and seismic stations. Geophys Res Lett 32:L17606. https://doi.org/10.1029/2005GL023783

Harms J, Ampuero JP, Barsuglia M, Chassande-Mottin E, Montagner JP, Somala SN, Whiting BF (2015) Transient gravity perturbations induced by earthquake rupture. Geophys J Int 201(3):1416–1425. https://doi.org/10.1093/gji/ggv090

Hayashi Y (2010) Empirical relationship of tsunami height between offshore and coastal stations. Earth Planets Space 62:269–275. https://doi.org/10.5047/eps.2009.11.006

Heaton TH (1975) Tidal triggering of earthquakes. Geophys J Int 43(2):307–326. https://doi.org/10.1111/j.1365-246X.1975.tb00637.x

Heidarzadeh M, Ishibe T, Gusman AR, Miyazaki H (2024) Field surveys of tsunami runup and damage following the January 2024 M_W 7.5 Noto (Japan sea) tsunamigenic earthquake. Ocean Eng 307:118140. https://doi.org/10.1016/j.oceaneng.2024.118140

Hendin G, Stiassnie M (2013) Tsunami and acoustic-gravity waves in water of constant depth. Phys Fluids 25(8):086103. https://doi.org/10.1063/1.4817996

Hickey MP, Schubert G, Walterscheid RL (2009) Propagation of Tsunami-driven gravity waves into the thermosphere and ionosphere. J Geophys Res Space Phys 114(A8):1. https://doi.org/10.1029/2009JA014105

Hill DP, Prejean SG (2007) Dynamic triggering. In: Kanamori H (ed) Earthquake seismology, treatise on geophysics, vol 4. Elsevier, Amsterdam, pp 257–291

Holgate SJ, Matthews A, Woodworth PL, Rickards LJ, Tamisiea ME, Bradshaw E, Foden PR, Gordon KM, Jevrejeva S, Pugh J (2013) New data systems and products at the permanent service for mean sea level. J Coastal Res 29(3):493–504. https://doi.org/10.2112/JCOASTRES-D-12-00175.1

Hong T-K, Wu R-S (2005) Scattering of elastic waves in geometrically anisotropic random media and its implication to sounding of heterogeneity in the earth's deep interior. Geophys J Int 163(1):324–338. https://doi.org/10.1111/j.1365-246X.2005.02760.x

Hong T-K, Wu R-S, Kennett BLN (2005) Stochastic features of scattering. Phys Earth Planet Inter 148(2–4):131–148. https://doi.org/10.1016/j.pepi.2004.08.002

Hong T-K, Choi E, Park S, Shin JS (2016) Prediction of ground motion and dynamic stress change in Baekdusan (Changbaishan) volcano caused by a North Korean nuclear explosion. Sci Rep 6(1):21477. https://doi.org/10.1038/srep21477

Hong T-K, Lee J, Chi D, Park S (2017) Seismic velocity changes in the backarc continental crust after the 2011 m_w9.0 Tohoku-Oki megathrust earthquake. Geophys Res Lett 44:10997–11003. https://doi.org/10.1002/2017GL075447

Hong T-K, Lee J, Park S, Kim W (2018) Time-advanced occurrence of moderate-size earthquakes in a stable intraplate region after a megathrust earthquake and their seismic properties. Sci Rep 8(1):13331. https://doi.org/10.1038/s41598-018-31600-5

Hong T-K, Park S, Lee J, Kim W (2020) Spatiotemporal seismicity evolution and seismic hazard potentials in the western east sea (sea of Japan). Pure Appl Geophys 177(8):3761–3774. https://doi.org/10.1007/s00024-020-02479-z

Hong T-K, Chung D, Lee J, Park S, Kim B, Kim W (2021a) Earthquake-spawning faults in the Seoul metropolitan area and their seismic implications. Earth Space Sci 8(7):e2021EA001662. https://doi.org/10.1029/2021EA001662

Hong T-K, Kim I, Park S, Kil D (2021b) Elastogravity waves and dynamic ground motions in the Korean Peninsula generated by the 11 March 2011 M_W9.0 Tohoku-Oki megathrust earthquake. J Geophys Res Solid Earth 126(2):e2020JB020628. https://doi.org/10.1029/2020JB020628

Hong T-K, Park S, Lee J, Lee J, Kim B (2024) Middle to lower crustal earthquakes in the western east sea (sea of Japan) and their implications for neotectonic evolution. Tectonophysics 880:230346. https://doi.org/10.1016/j.tecto.2024.230346

Houng SE, Lee J, Hong T-K (2016) Dynamic seismic response of a stable intraplate region to a megathrust earthquake. Tectonophysics 689:67–78. https://doi.org/10.1016/j.tecto.2016.07.033

Janssen P (2004) The interaction of ocean waves and wind. Cambridge University Press, Cambridge

Jo E, Hong T-K (2013) Vp/vs ratios in the upper crust of the southern Korean peninsula and their correlations with seismic and geophysical properties. J Asian Earth Sci 66:204–214. https://doi.org/10.1016/j.jseaes.2013.01.008

Kanamori H (1972) Mechanism of tsunami earthquakes. Phys Earth Planet Int 6(5):346–359. https://doi.org/10.1016/0031-9201(72)90058-1

Kennett B (2009) Seismic wave propagation in stratified media, ANU Press, p 288

Kim I, Hong T-K (2018) Azimuthal seismic anisotropy in the upper crust of the Japanese islands induced by the 2011 Tohoku-Oki megathrust earthquake. Geophys Res Lett 45:12793–12803. https://doi.org/10.1029/2018GL080742

Kim B, Hong T-K (2022) A national V_{S30} model for South Korea to combine nationwide dense borehole measurements with ambient seismic noise analysis. Earth Space Sci 9(1):e2021EA002066. https://doi.org/10.1029/2021EA002066

Kimura T, Tanaka S, Saito T (2013) Ground tilt changes in Japan caused by the 2010 Maule, Chile, earthquake tsunami. J Geophys Res Solid Earth 118(1):406–415. https://doi.org/10.1029/2012JB009657

Kinoshita S (2008) Tilt measurement using broadband velocity seismograms. Bull Seismol Soc Am 98(4):1887–1897. https://doi.org/10.1785/0120070230

Kobori T, Takahashi M, Nasu T, Niwa N, Ogasawara K (1993) Seismic response controlled structure with active variable stiffness system. Earthqu Eng Struct Dyn 22(11):925–941. https://doi.org/10.1002/eqe.4290221102

Korn M (1993) Seismic waves in random media. J Appl Geophys 29(3–4):247–269. https://doi.org/10.1016/0926-9851(93)90007-L

Kubota T, Saito T, Chikasada NY, Suzuki W (2020) Ultrabroadband seismic and tsunami wave observation of high.sampling.ocean bottom pressure gauge covering periods from seconds to hours. Earth Space Sci 7:e2020EA001197. https://doi.org/10.1029/2020EA001197

Kutschera F, Jia Z, Oryan B, Wong JWC, Fan W, Gabriel AA (2024) The multi-segment complexity of the 2024 M_W 7.5 Noto Peninsula Earthquake governs tsunami generation. Geophys Res Lett 51(21):e2024GL109790. https://doi.org/10.1029/2024GL109790

Laurendeau A, Cotton F, Ktenidou OJ, Bonilla LF, Hollender F (2013) Rock and stiff-soil site amplification: dependency on v_{s30} and kappa (κ_0). Bull Seismol Soc Am 103(6):3131–3148. https://doi.org/10.1785/0120130020

Lee HS, Kim KO, Yamashita T, Komaguchi T, Mishima T (2010) Abnormal storm waves in the winter east/Japan sea: generation process and hindcasting using an atmosphere-wind wave modelling system. Nat Hazard 10(4):773–792. https://doi.org/10.5194/nhess-10-773-2010

Lee EJ, Kim K, Park JH (2022) Reconstruction of long-term sea-level data gaps of tide gauge records using a neural network operator. Front Mar Sci 9:1037697. https://doi.org/10.3389/fmars.2022.1037697

Levin BW, Nosov M (2009) Physics of Tsunamis, vol 327. Springer, Dordrecht

Liu L, Dobry R (1997) Seismic response of shallow foundation on liquefiable sand. J Geotech Geoenviron Eng 123(6):557–567. https://doi.org/10.1061/(ASCE)1090-0241(1997)123:6(557)

Longuet-Higgins MS (1950) A theory of the origin of microseisms, philosophical transactions of the royal society of London. Ser A Math Phys Sci 243(857):1–35. https://doi.org/10.1098/rsta.1950.0012

Ma Z, Zeng H, Luo H, Liu Z, Jiang Y, Aoki Y, Wang W, Itoh Y, Lyu M, Cui Y, Yun SH, Hill EM, Wei S (2024) Slow rupture in a fluid-rich fault zone initiated the 2024 M_W 7.5 Noto earthquake. Science 385(6711):866–871. https://doi.org/10.1126/science.ado5143

Masuda H, Sugawara D, Cheng AC, Suppasri A, Shigihara Y, Kure S, Imamura F (2024) Modeling the 2024 Noto peninsula earthquake tsunami: implications for tsunami sources in the eastern margin of the Japan sea. Geosci Lett 11(1):29. https://doi.org/10.1186/s40562-024-00344-8

McKenzie D, Jackson J (2012) Tsunami earthquake generation by the release of gravitational potential energy. Earth Planet Sci Lett 345:1–8. https://doi.org/10.1016/j.epsl.2012.06.036

Merrifield MA, Firing YL, Aarup T, Agricole W, Brundrit G, Chang-Seng D, Farre R, Kilonsky B, Knight W, Kong L, Magori C, Manurung P, McCreery C, Mitchell W, Pillay S, Schindele F, Shillington F, Testut L, Wijeratne EMS, Caldwell P, Jardin J, Nakahara S, Porter F-Y, Turetsky N (2005) Tide gauge observations of the Indian ocean tsunami, December 26, 2004. Geophys Res Lett 32:L09603. https://doi.org/10.1029/2005GL022610

Mikumo T, Garces M, Shibutani T, Morii W, Okawa T, Ishihara Y (2013) Acoustic-gravity waves from the source region of the 2011 great Tohoku earthquake (M_W=9.0). J Geophys Res Solid Earth 118(4):1534–1545. https://doi.org/10.1002/jgrb.50143

Miyazawa M, Brodsky EE, Guo H (2021) Dynamic earthquake triggering in southern California in high resolution: intensity, time decay, and regional variability. AGU Adv 2:e2020AV000309. https://doi.org/10.1029/2020AV000309

Montagner JP, Juhel K, Barsuglia M, Ampuero JP, Chassande-Mottin E, Harms J, Whiting B, Bernard P, Clévédé E, Lognonné P (2016) Prompt gravity signal induced by the 2011 Tohoku-Oki earthquake. Nat Commun 7(1):1–7. https://doi.org/10.1038/ncomms13349

Mulia IE, Ishibe T, Satake K, Gusman AR, Murotani S (2020) Regional probabilistic tsunami hazard assessment associated with active faults along the eastern margin of the sea of Japan. Earth Planets Space 72:1–15. https://doi.org/10.1186/s40623-020-01256-5

Nawa K, Suda N, Satake K, Fujii Y, Sato T, Doi K, Kanao M, Shibuya K (2007) Loading and gravitational effects of the 2004 Indian ocean tsunami at Syowa station. Antarc Bull Seismol Soc Am 97(1A):S271–S278. https://doi.org/10.1785/0120050625

Nishida K, Maeda T, Fukao Y (2019) Seismic observation of tsunami at island broadband stations. J Geophys Res Solid Earth 124:1910–1928. https://doi.org/10.1029/2018JB016833
Nishikawa Y, Yamamoto MY, Nakajima K, Hamama I, Saito H, Kakinami Y, Yamada M, Ho TC (2022) Observation and simulation of atmospheric gravity waves exciting subsequent tsunami along the coastline of Japan after Tonga explosion event. Sci Rep 12(1):22354. https://doi.org/10.1038/s41598-022-25854-3
Oh SH, Jeong WM (2013) Characteristics of high waves observed at multiple stations along the east coast of Korea. Nat Hazard 13(12):3503–3514. https://doi.org/10.5194/nhess-13-3503-2013
Okal EA (1988) Seismic parameters controlling far-field tsunami amplitudes: a review. Nat Hazards 1:67–96. https://doi.org/10.1007/BF00168222
Okal EA (2007) Seismic records of the 2004 Sumatra and other tsunamis: a quantitative study. Pure Appl Geophys 164:325–353. https://doi.org/10.1007/s00024-006-0181-4
Okal EA (2017) The excitation of tsunamis by deep earthquakes. Geophys J Int 209(1):234–249. https://doi.org/10.1093/gji/ggx013
Okal EA, Synolakis CE (2003) A theoretical comparison of tsunamis from dislocations and landslides. Pure Appl Geophys 160(10):2177–2188. https://doi.org/10.1007/s00024-003-2425-x
Okuwaki R, Yagi Y, Murakami A, Fukahata Y (2024) A multiplex rupture sequence under complex fault network due to preceding earthquake swarms during the 2024 M_W 7.5 Noto Peninsula, Japan, earthquake. Geophys Res Lett 51(11):e2024GL109224. https://doi.org/10.1029/2024GL109224
Park S, Hong TK (2020) Typhoon-induced microseisms around the south China sea. Seismol Soc Am 91(6):3454–3468. https://doi.org/10.1785/0220190310
Park S, Hong T-K (2024) Continent-side uplifted mantle and geological imprints along a paleo rift in the western East Sea (Sea of Japan). J Geophys Res Solid Earth 129:e2024JB029049. https://doi.org/10.1029/2024JB029049
Park S, Hong T-K, Rah G (2021) Seismic hazard assessment for the Korean Peninsula. Bull Seismol Soc Am 111(5):2696–2719. https://doi.org/10.1785/0120200261
Park S, Hong T-K, Kim B, Lee J (2023) Role of backbone fault system on earthquake spawning and geohazards in the Seoul metropolitan area. Earth Space Sci 10(3):e2022EA002686. https://doi.org/10.1029/2022EA002686
Pelayo AM, Wiens DA (1992) Tsunami earthquakes: slow thrust-faulting events in the accretionary wedge. J Geophys Res Solid Earth 97(B11):15321–15337. https://doi.org/10.1029/92JB01305
Pino NA, Ripepe M, Cimini GB (2004) The Stromboli volcano landslides of December 2002: a seismological description. Geophys Res Lett 31(2):1. https://doi.org/10.1029/2003GL018385
Poplavskiy AS, Bras RJ (2013) Recordings of long-period fluctuations associated with the passage of three distinct tsunamis at broadband seismometers made at the international monitoring system (IMS) hydroacoustic t-station h06 (Socorro island, Mexico). Seismol Res Lett 84(4):567–578. https://doi.org/10.1785/0220120116
Rabinovich AB, Eblé MC (2015) Deep-ocean measurements of tsunami waves. Pure Appl Geophys 172(12):3281–3312. https://doi.org/10.1007/s00024-015-1058-1
Rabinovich AB, Thomson RE, Stephenson FE (2006) The Sumatra tsunami of 26 December 2004 as observed in the north pacific and north Atlantic oceans. Surv Geophys 27(6):647–677. https://doi.org/10.1007/s10712-006-9000-9
Rolland LM, Occhipinti G, Lognonne P, Loevenbruck A (2010) Ionospheric gravity waves detected offshore Hawaii after tsunamis. Geophys Res Lett 37(17):1. https://doi.org/10.1029/2010GL044479
Saito T (2019) Tsunami generation and propagation. Springer, Tokyo, p p265
Satake K (1985) The mechanism of the 1983 Japan sea earthquake as inferred from long-period surface waves and tsunamis. Phys Earth Planet Int 37(4):249–260
Satake K (1994) Mechanism of the 1992 Nicaragua tsunami earthquake. Geophys Res Lett 21(23):2519–2522
Satake K (2002) Tsunamis. In: International geophysics, vol 81, Academic press, New York, pp 437–451
Satake K, Tanioka Y (1995) Tsunami generation of the 1993 Hokkaido Nansei-Oki earthquake. Pure Appl Geophys 144(3):803–821. https://doi.org/10.1007/BF00874395
Satake K, Tanioka Y (1999) Sources of tsunami and tsunamigenic earthquakes in subduction zones. Pure Appl Geophys 154:467–483. https://doi.org/10.1007/s000240050240
Satake K, Ishibe T, Murotani S, Mulia IE, Gusman AR (2022) Effects of uncertainty in fault parameters on deterministic tsunami hazard assessment: examples for active faults along the eastern margin of the sea of Japan. Earth Planets Space 74(1):36. https://doi.org/10.1186/s40623-022-01594-6
Sato H, Shimamoto T, Tsutsumi A, Kawamoto E (1995) Onshore tsunami deposits caused by the 1993 southwest Hokkaido and 1983 Japan sea earthquakes. Pure Appl Geophys 144:693–717. https://doi.org/10.1007/978-3-0348-7279-9_18

Seyhan E, Stewart JP (2014) Semi-empirical nonlinear site amplification from NGA-west2 data and simulations. Earthq Spectra 30(3):1241–1256. https://doi.org/10.1193/063013EQS181M
Shuto N, Matsutomi H (1995) Field survey of the 1993 Hokkaido Nansei-Oki earthquake tsunami. Pure Appl Geophys 144:649–663. https://doi.org/10.1007/BF00874388
Sohn YJ, Kim KH, Kang SY, Kim D, Lee YC (2023) Seismic noise characteristics of PNU OBS network in 2021–2022. In EGU general assembly conference abstracts, pp EGU-5838
Stewart JP, Parker GA, Atkinson GM, Boore DM, Hashash YM, Silva WJ (2020) Ergodic site amplification model for central and eastern north America. Earthq Spectra 36(1):42–68. https://doi.org/10.1177/8755293019878185
Synolakis CE (1987) The runup of solitary waves. J Fluid Mech 185:523–545. https://doi.org/10.1017/S002211208700329X
Synolakis CE, Okal EA (2005) 1992–2002: perspective on a decade of post-tsunami surveys. Tsunamis: case studies and recent developments. Springer, Dordrecht, pp 1–29
Tadepalli S, Synolakis CE (1994) The run-up of N-waves on sloping beaches. Proc R Soc Lond Ser A Math Phys Sci 445(1923):99–112. https://doi.org/10.1098/rspa.1994.0050
Takahashi T, Takahashi T, Shuto N, Imamura F, Ortiz M (1995) Source models for the 1993 Hokkaido Nansei-Oki earthquake tsunami. Pure Appl Geophys 144:747–767. https://doi.org/10.1007/BF00874393
Takeda Y, Enescu B, Miyazawa M, An L (2024) Dynamic triggering of earthquakes in northeast Japan before and after the 2011 M 9.0 Tohoku-Oki earthquake. Bull Seismol Soc Am 114(4):1884–1901. https://doi.org/10.1785/0120230051
Tanaka S, Ohtake M, Sato H (2002) Evidence for tidal triggering of earthquakes as revealed from statistical analysis of global data. J Geophys Res Solid Earth 107(B10):2211. https://doi.org/10.1029/2001JB001577
Tanioka Y, Satake K, Ruff L (1995) Total analysis of the 1993 Hokkaido Nansei-Oki earthquake using seismic wave, tsunami, and geodetic data. Geophys Res Lett 22(1):9–12. https://doi.org/10.1029/94GL02787
Titov VV, Synolakis CE (1997) Extreme inundation flows during the Hokkaido-Nansei-Oki tsunami. Geophys Res Lett 24(11):1315–1318. https://doi.org/10.1029/97GL01128
Titov VV, Synolakis CE (1998) Numerical modeling of tidal wave runup. J Waterw Port Coast Ocean Eng 124(4):157–171. https://doi.org/10.1061/(ASCE)0733-950X(1998)124:4(157)
Titov V, Rabinovich AB, Mofjeld HO, Thomson RE, Gonzalez FI (2005) The global reach of the 26 December 2004 Sumatra Tsunami. Science 309(5743):2045–2048. https://doi.org/10.1126/science.1114576
Todorovska MI, Trifunac MD (2001) Generation of tsunamis by a slowly spreading uplift of the sea floor. Soil Dyn Earthq Eng 21(2):151–167. https://doi.org/10.1016/S0267-7261(00)00096-8
Vallée M, Ampuero JP, Juhel K, Bernard P, Montagner JP, Barsuglia M (2017) Observations and modeling of the elastogravity signals preceding direct seismic waves. Science 358(6367):1164–1168. https://doi.org/10.1126/science.aao0746
Van der Elst NJ, Brodsky EE (2010) Connecting near-field and far-field earthquake triggering to dynamic strain. J Geophys Res 115(B7):1. https://doi.org/10.1029/2009JB006681
Wapenaar K, Fokkema J (2006) Green's function representations for seismic interferometry. Geophysics 71(4):SI33–SI46. https://doi.org/10.1190/1.2213955
Ward SN (1980) Relationships of tsunami generation and an earthquake source. J Phys Earth 28(5):441–474. https://doi.org/10.4294/jpe1952.28.441
Webb SC (2002) Seismic noise on land and on the sea floor. In: Lee WHK, Kanamori H, Jennings PC, Kisslinger C (eds) International handbook on earthquake and engineering seismology, part A, chapter 19. Academic Press, Amsterdam, pp 305–318
Wielandt E (2002) Seismometry. In: Lee WHK, Kanamori H, Jennings PC, Kisslinger C (eds) International handbook on earthquake and engineering seismology, part A, chapter 18. Academic Press, Amsterdam, pp 283–304
Wielandt E, Forbriger T (1999) Near-field displacement and tilt associated with the explosive activity of Stromboli. Annali di Geofiscia 42(3):407–416. https://doi.org/10.4401/ag-3723
Woodworth PL, Player R (2003) The permanent service for mean sea level: an update to the 21st century. J Coast Res 1:287–295
Xu L, Ji C, Meng L, Ampuero JP, Yunjun Z, Mohanna S, Aoki Y (2024) Dual-initiation ruptures in the 2024 Noto earthquake encircling a fault asperity at a swarm edge. Science 385(6711):871–876. https://doi.org/10.1126/science.adp0493

Yamanaka Y, Matsuba Y, Shimozono T, Tajima Y (2024) Nearshore propagation and amplification of the Tsunami following the 2024 Noto Peninsula Earthquake. Jpn Geophys Res Lett 51(19):e2024GL110231. https://doi.org/10.1029/2024GL110231

Yan R, Chen X, Sun H, Xu J, Zhou J (2023) A review of tidal triggering of global earthquakes. Geodesy Geodyn 14(1):35–42. https://doi.org/10.1016/j.geog.2022.06.005

Yang S, Sang C, Hu Y, Wang K (2024) Coseismic and early postseismic deformation of the 2024 M_W 7.45 Noto Peninsula Earthquake. Geophys Res Lett 51(11):e2024GL108843. https://doi.org/10.1029/2024GL108843

Yu Y, Yan Z, Hickey MP (2015) Lower thermospheric response to atmospheric gravity waves induced by the 2011 Tohoku Tsunami. J Geophys Res Space Phys 120(6):5062–5075. https://doi.org/10.1002/2015JA020986

Yuan X, Kind R, Pedersen HA (2005) Seismic monitoring of the Indian Ocean Tsunami. Geophys Res Lett 32:L15308. https://doi.org/10.1029/2005GL023464

Yuhi M, Umeda S, Arita M, Ninomiya J, Gokon H, Arikawa T, Baba T, Imamura F, Kawai A, Kumagai K, Kure S, Miyashita T, Suppasri A, Nobuoka H, Shibayama T, Koshimura S, Mori N (2024) Post-event survey of the 2024 Noto Peninsula earthquake Tsunami in Japan. Coast Eng J 66(3):405–418. https://doi.org/10.1080/21664250.2024.2368955